ELSEVIER

Journal of Biomechanics 40 (2007) 1310–1317

JOURNAL OF BIOMECHANICS

www.elsevier.com/locate/jbiomech
www.JBiomech.com

Geometry of human ribs pertinent to orthopedic chest-wall reconstruction

Marcus Mohr, Eduard Abrams, Christine Engel, William B. Long, Michael Bottlang*

Biomechanics Laboratory, Legacy Research and Technology Center, 1225 NE 2nd Avenue, Portland, OR 97232, USA

Accepted 17 May 2006

Abstract

Orthopedic reconstruction of blunt chest trauma can aid restoration of pulmonary function to reduce the mortality associated with serial rib fractures and flail chest injuries. Contemporary chest wall reconstruction requires contouring of generic plates to the complex surface geometry of ribs. This study established a biometric foundation to generate specialized, anatomically contoured osteosynthesis hardware for rib fracture fixation. On human cadaveric ribs three through nine, the surface geometry pertinent to anatomically conforming osteosynthesis plates was characterized by quantifying the apparent rib curvature C_A, the longitudinal twist α_{LT} along the diaphysis, and the unrolled curvature C_U. In addition, the rib cross-sectional geometry pertinent to intramedullary fixation strategies was characterized in terms of cross-section height, width, area, and cortex thickness. The rib surface exhibited a curvature C_A ranging from 3.8 m^{-1} in the anteromedial section of rib seven to 17.3 m^{-1} in the posterior section of rib three. All ribs had in common a longitudinal twist α_{LT}, ranging from 41–60°. The unrolled curvature C_U decreased gradually from ribs three to five, and increased gradually with reversed orientation from rib six to nine. The cross-sectional area remained constant along the rib diaphysis. However, the medullary canal increased in size from 29.9 mm^2 posteriorly to 41.2 mm^2 in anterior rib segments. Results of this biometric rib characterization describe a novel strategy for intraoperative plate contouring and provide a foundation for the development of specialized rib osteosynthesis strategies.

Keywords: Rib; Reconstruction; Geometry; Cross-sectional shape

1. Introduction

Rib fractures are present in 4–10% of trauma patients admitted to hospitals (Mayberry and Trunkey, 1997). About 10% of chest traumata result in a flail chest (Lardinois et al., 2001), defined as segmental facture of at least four consecutive ribs. Flail chest injury is associated with a mortality rate of 10–36% (Cacchione et al., 2000; Hellberg et al., 1981; Labitzke, 1981; Landercasper et al., 1984; Lardinois et al., 2001; Schmit-Neuerburg et al., 1982). In flail chest injuries, paradoxical inward movement of the flail segment prevents effective inspiration and requires prolonged mechanical ventilation, which in turn can lead to pneumonia and sepsis (Labitzke, 1981; Lardinois et al., 2001; Mouton et al., 1997; Tanaka et al., 2002; Tscharner et al., 1989).

Operative fixation of multiple segmental rib fractures can accelerate restoration of pulmonary function (Ahmed and Mohyuddin, 1995; Haasler, 1990; Labitzke et al., 1980; Tanaka et al., 2002; Tscharner et al., 1989; Voggenreiter et al., 1998; Voggenreiter et al., 1996), shorten ICU stay and hospitalization (Ahmed and Mohyuddin, 1995; Haasler, 1990; Tanaka et al., 2002), and reduce mortality associated with prolonged mechanical ventilation (Balci et al., 2004; Karev, 1997; Labitzke, 1981; Landreneau et al., 1991; Lardinois et al., 2001; Quell and Vecsei, 1991; Tanaka et al., 2002; Tscharner et al., 1989; Velmahos et al., 2002). A further benefit of operative chest wall stabilization is a

*Corresponding author. Tel.: +503 413 5457; fax: +503 413 5216.
E-mail address: mbottlang@biomechresearch.org (M. Bottlang).

0021-9290/$ - see front matter © 2006 Elsevier Ltd. All rights reserved.
doi:10.1016/j.jbiomech.2006.05.017

decreased likelihood of clinically significant long-term respiratory dysfunction and skeletal deformity (Haasler, 1990; Meier and Schuepbach, 1978).

Despite the potentially live-saving intervention, no specialized hardware for rib reconstruction is commercially available today. Early plate designs for rib fixation were straight and required intraoperative contouring (Borrely et al., 1985; Martin et al., 1982; Menard et al., 1983; Vecsei et al., 1979). Today, generic small fracture plates are most commonly used for rib fracture fixation (Engel et al., 2005; Friedrich et al., 1991; Lardinois et al., 2001; Mouton et al., 1997; Ng et al., 2001; Oyarzun et al., 1998; Reber et al., 1993). However, due to the complex geometry of ribs, intraoperative contouring of generic plates is time-consuming and difficult at best. Furthermore, the use of generic plates with vastly varying mechanical and geometric properties is accompanied by a high incidence of screw loosening and pullout (Boetsch and Rehm, 1981; Friedrich et al., 1991; Hellberg et al., 1981; Mouton et al., 1997; Voggenreiter et al., 1996). As holds true for precontoured osteosynthesis plates in general, anatomically conforming rib plates will likely improve anatomic reduction and stability, significantly shorten the operation time, and consequently decrease the risk of infection.

As a less-invasive alternative to plate osteosynthesis, Kirschner wires for intramedullary fixation have been used (Quell and Vecsei, 1991). Intramedullary fixation is especially attractive for posterior rib fractures that are not amenable for plate fixation due to lack of surgical accessibility. However, the circular cross-section of Kirschner wires provides little rotational stability and lack of secure fixation inside the canal can lead to wire migration (Ahmed and Mohyuddin, 1995; Albrecht and Brug, 1979; Meier and Schuepbach, 1978; Moore, 1975; Vecsei et al., 1979). Akin to standard practice for intramedullary fixation, knowledge of the medullary canal geometry in ribs will be crucial to select a properly dimensioned intramedullary fixation device.

Most recently, Engel et al. (2005) concluded that further research is necessary to design specific fixation hardware which takes into account the structural properties, geometry, and fixation constraints of ribs.

While rib cage dimensions have been obtained with several techniques (Fick et al., 1911; Fujimoto et al., 1984; Nussbaum and Chaffin, 1996), a comprehensive description of the geometric properties of individual ribs is not available to date. Most pertinent to plate fixation, no study has described the barrel-shaped outer surface of the human rib cage to which plates have to be contoured intraoperatively. The cross-sectional geometry of human ribs has been quantified for the mid-diaphyseal region only, without examining changes thereof along the rib (Stein and Granik, 1976; Takahashi and Frost, 1966; Yoganandan and Pintar, 1998).

This study quantified the longitudinal geometry of human ribs in terms of their spatial surface geometry in order to aid development of anatomically contoured plating hardware. In addition, the cross-sectional geometry along ribs was quantified as a morphometric basis for the advancement of intramedullary fixation alternatives.

2. Method

This laboratory study evaluated the geometry of human cadaveric ribs three through nine. The first part of this study examined the longitudinal geometry of ribs by quantifying the apparent rib curvature, the longitudinal twist along the diaphysis, and the unrolled curvature of the outer cortical surface. The second part of this study investigated the cross-sectional geometry of ribs over their length by measuring the height and width of each cross-section, the cortical thickness, and the area of the cortex and the medullary canal.

2.1. Longitudinal rib geometry

Right ribs 3–9 were harvested from eight fresh frozen human cadavers (64 ± 13 yr, 172 ± 10 cm, 64 ± 25 kg, 4 male, 4 female) and stripped of soft tissue. Three parallel lines l_M, l_S, l_I were marked along each rib's outer surface between the tubercle and the costo-chondral junction (CCJ) at mid-height, 5 mm superior and 5 mm inferior of mid-height, respectively (Fig. 1). A reference frame was defined for each rib with the origin in the center of the tubercle, the y-axis intersecting the CCJ, and the x–y-plane coinciding with the midline l_m at 0% (tubercle), 50%, and 100% (CCJ) of the rib length. Points $P_{S,i}$, $P_{M,i}$, and $P_{I,i}$ were digitized in 2 mm intervals along lines l_S, l_M, and l_I, respectively, using a three-dimensional digitizing system with an accuracy of ±0.12 mm (MicroScribe G2, Immersion, San Jose, CA).

2.1.1. Apparent rib curvature C_a

Three non-collinear points distributed along a curve segment define a unique circle in space with an apparent radius vector $\vec{R}_A$ (Fig. 1a). The apparent radius $\vec{R}_A$ along the rib was calculated by fitting circles to sequential point triplets ($P_{M,i-20}$, $P_{M,i}$, $P_{M,i+20}$), using custom software code (MATLAB, The MathWorks, Natick, MA). The apparent curvature magnitude was then expressed as $C_A = 1/R_A$ for normalized locations from 15% to 85% of rib length (0% = tubercle, 100% = CCJ).

2.1.2. Longitudinal twist α_{LT}

Ribs 3–9 have in common a characteristic twist about their longitudinal axis. This twist was quantified by calculating angles α_i between the orientation of the outer cortical surface, defined by vectors $\overrightarrow{P_I P_S}$, and unit vector

$\vec{e}_Z$, which is parallel to the z-axis (Fig. 1b). The total longitudinal twist α_{LT} was defined as the difference between α_i values obtained at 15% and 85% of the rib length.

2.1.3. Unrolled curvature C_u

The outer surface of the rib was unrolled onto a plane (Fig. 1c), in order to derive a two-dimensional shape that, upon bending to the apparent rib curvature C_A, follows the outer surface of the rib. This was realized by outlining the rib contour on a flexible sheet conformed to the rib's outer surface. Subsequently, this sheet was unrolled on a flat surface and the curvature C_u of the centerline was computed for the segment from 15% to 85% rib length.

2.2. Cross-sectional rib geometry

The cross-sectional geometry of ribs 3–9 from five fresh frozen human cadavers was examined (59 ± 13 yr, 71 ± 30 kg, 3 male, 2 female). Using a circular saw with a diamond blade, 2-mm thick cross-sections were excised at 5%, 25%, 50%, and 75% of rib length (Fig. 2a). The rib length was defined from the tubercle (0%) to the CCJ (100%) in each rib. The 5% cross-section was located between the tubercle and angle. Contact radiographs of cross-sectional specimens were obtained, whereby specimens were aligned with the cortical surface vector $\overrightarrow{P_I P_S}$ parallel to the edge of the X-ray cassette. For quantitative image analysis with MATLAB, the radiographs were scanned in 8-bit grayscale mode at 0.03 mm resolution. Successive gray scale equalization and thresholding were applied to objectively extract cortical and trabecular structures. Three features were quantified:

2.2.1. Cross-sectional height and width

A bounding box was fitted to each cross-sectional image, with the side lengths of the box representing the height (h) and width (w) of each cross-section (Fig. 2b).

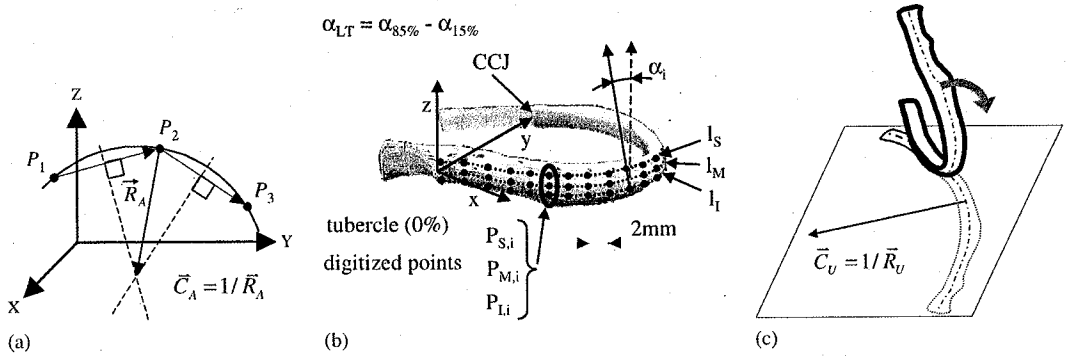

Fig. 1. Longitudinal rib geometry: assessment of (a) the apparent curvature C_A along the rib; (b) the longitudinal twist α_{LT}, shown in reference to the rib coordinate system; and (c) the unrolled curvature C_U.

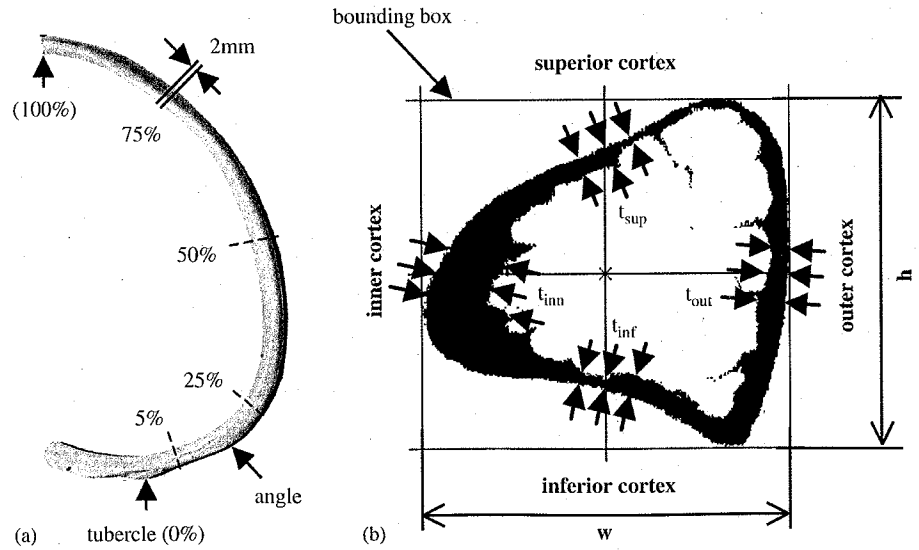

Fig. 2. Cross-sectional rib geometry: (a) location of cross sections and (b) discretized contact radiograph of rib slice for assessment of cross-section height (h), width (w), area, and cortex thickness (t).

2.2.2. Cortex thickness t_C

The cortex thickness t_C was measured at the intersections of the cortex with the horizontal and vertical symmetry lines of the bounding box of each cross-section (Fig. 2b). In addition, t_C was also measured 0.75 mm before and after each intersection to obtain average t_C reports of the superior (t_{sup}), inferior (t_{inf}), inner (t_{inn}), and outer (t_{out}) cortex over 1.5-mm regions of interest.

2.2.3. Cross-sectional area A

The total area A_T and the cortex area A_C of each cross-section were computed. The area of the medullary canal A_M was calculated by subtracting the cortex area from the total cross-sectional area.

The accuracy of cross-sectional measurements was determined by the 0.03-mm resolution of the quantitative image analysis procedure. The accuracy of C_A assessment was evaluated by digitizing the perimeter of a circle with 150 mm radius in 2-mm increments. The accuracy of α_{LT} assessment was determined theoretically, by perturbing raw data for α_{LT} calculation with a maximal digitizing error of 0.5 mm.

All outcome parameters are presented by their mean value $\pm$ one standard deviation. Where applicable, statistically significant differences were determined using a one-way ANOVA and Tukey's HSD post-hoc test at an α-level of 0.05.

3. Results

3.1. Longitudinal rib geometry

The *apparent rib curvature* C_A varied along the length of individual ribs and between ribs of different anatomical levels (Fig. 3). Among ribs three through nine, C_A was most consistent at 15% ($C_{A,15\%} = 15.2$–$17.3\,m^{-1}$) and 85% ($C_{A,85\%} = 6.2$–$8.0\,m^{-1}$). Among all ribs, the highest curvature was found posterior at 15% rib length, with rib three exhibiting the highest overall curvature of $C_{A,15\%} = 17.3 \pm 1.7\,m^{-1}$. The curvature of ribs three and four decreased from posterior to anterior and was on average smallest at 85% rib length. Rib five reached its smallest average curvature at 75% length, ribs six and seven at 65%, and ribs eight and nine at 55%. The straightest segment was found in rib seven at 65% length with $C_{A,65\%} = 3.8 \pm 1.5\,m^{-1}$. Accuracy assessment of C_A by digitization of five point triplets on the 150-mm radius calibration circle yielded a C_A value of 149.5 ± 3.1 mm.

The *longitudinal twist* α_{LT} was a characteristic feature common to all ribs. It was found to be counterclockwise in all specimens. The average magnitude of α_{LT} was notably consistent between ribs 3–7 (range 41 ± 14–$44.8 \pm 16.9°$) and was over 30% higher in ribs eight and nine ($60.1 \pm 5.7°$ and $58.1 \pm 10.9°$, respectively), although no statistically significant difference in α_{LT} was found ($p > 0.05$). The maximal error in α_{LT} caused by source data perturbation was <4.3% for α_{LT} values of 40–60°.

The *unrolled curvature* C_U changed significantly ($p < 0.01$) and decreased in a quasi-linear fashion ($R = -0.96$) from rib 3–9 (Fig. 4). The direction of C_U in ribs 3–5 was opposite to the direction of C_U in ribs 6–9. C_U was most pronounced in rib three with a magnitude of $6.9 \pm 0.7\,m^{-1}$. C_U was smallest in rib six with $1.1\,m^{-1}$.

3.2. Cross-sectional rib geometry

The *cross-sectional height and width*, averaged for each of ribs 3–9 is depicted in Table 1. Within each rib, the

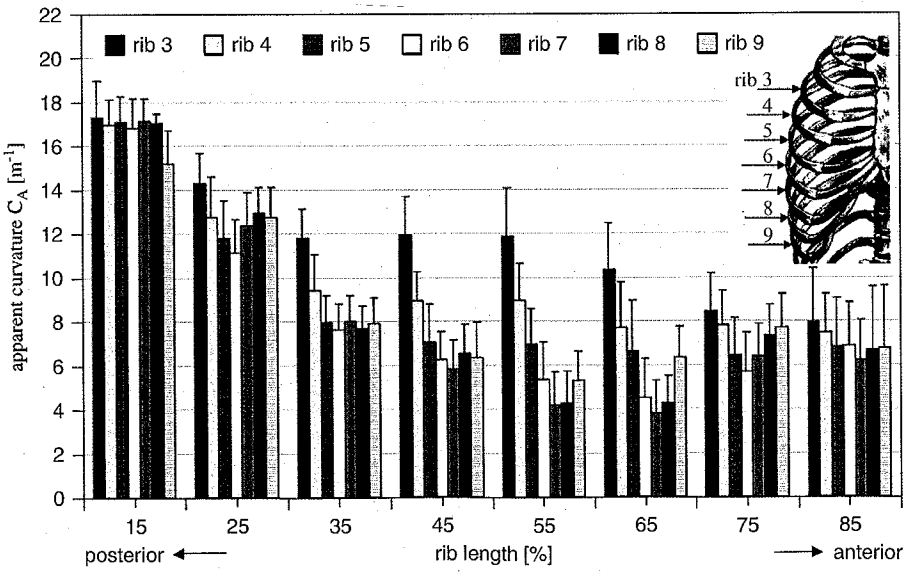

Fig. 3. Apparent rib curvature C_A for right ribs three through nine, depicted along each rib in 10% increments of length.

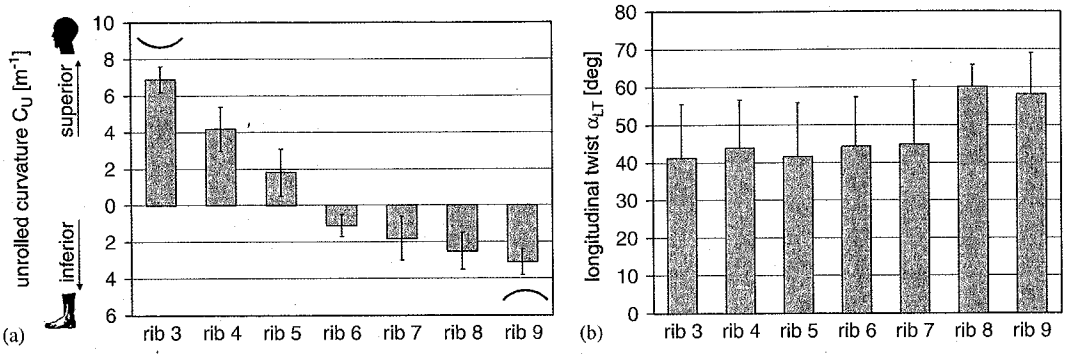

Fig. 4. (a) The unrolled curvature C_U decreased gradually from ribs three to five, and increased gradually with reversed orientation from rib 6–9 and (b) all ribs had in common a counterclockwise longitudinal twist α_{LT}.

Table 1
Outer dimension and cortex thickness in mm, averaged over entire rib length ($n = 20$)

	Rib 3	Rib 4	Rib 5	Rib 6	Rib 7	Rib 8	Rib 9
h	11.3±2.5	11.6±2.6	11.4±2.6	11.8±2.6	12.8±2.8	13.1±3.6	12.3±3.8
w	6.0±2.0	6.8±2.0	7.2±1.9	7.6±1.8	7.4±1.7	6.5±2.1	6.6±1.9
t_{inf}	0.5±0.3	0.5±0.3	0.5±0.3	0.5±0.3	0.5±0.2	0.6±0.4	0.6±0.4
t_{inn}	0.9±0.4	1.1±0.4	1.1±0.4	1.4±0.4	1.4±0.4	1.2±0.6	1.1±0.4
t_{sup}	0.6±0.4	0.6±0.5	0.4±0.3	0.5±0.3	0.5±0.3	0.6±0.4	0.6±0.3
t_{out}	0.7±0.3	0.7±0.3	0.8±0.4	0.9±0.5	0.9±0.4	0.8±0.4	0.8±0.4

cross-sectional dimension changed as a function of location. Averaged among all ribs, height h at 5%, 25%, 50%, and 75% locations was 10.4±1.8, 13.5±3.4, 12.3±3.0, and 12.0±2.9 mm, respectively. At the 5% location, h was significantly smaller than at the 25% location ($p<0.01$) and the 50% location ($p<0.05$). The average width w at 5%, 25%, 50%, and 75% was 7.5±1.8, 7.1±2.1, 6.9±2.1, and 5.9±1.5 mm, respectively. At the 75% location, w was significantly smaller than at the 5% location ($p<0.05$) and at the 25% location ($p<0.05$). The width-to-height ratio decreased from 0.7 posteriorly to 0.5 anteriorly, where ribs were twice as high as they were wide.

The *cortex thickness* for t_{inn}, t_{out}, t_{sup}, and t_{inf}, averaged for each of ribs three through nine is depicted in Table 1. Changes in cortex thickness along ribs are shown in Fig. 5, depicting the average cortex thickness among all ribs at 5%, 25%, 50%, and 75% locations. On average, t_{inn} was 1.1±0.5 mm, and 37.5% thicker than t_{out}. At the 25%, 50%, and 75% locations, t_{inn} was significantly thicker ($p<0.01$) than t_{out}. The average thickness of t_{out}, t_{sup}, and t_{inf} was 0.8±0.4 mm, 0.5±0.4 mm, and 0.5±0.3 mm, respectively.

The total *cross-sectional area* A_T, averaged for ribs three through nine, remained nearly constant along the rib length (Fig. 6). However, the average cortical area A_C decreased significantly from 26.3 mm^2 at 5% rib length to 16.3 mm^2 at 75% rib length ($p<0.05$). The medullary area A_M, on the other hand, increased

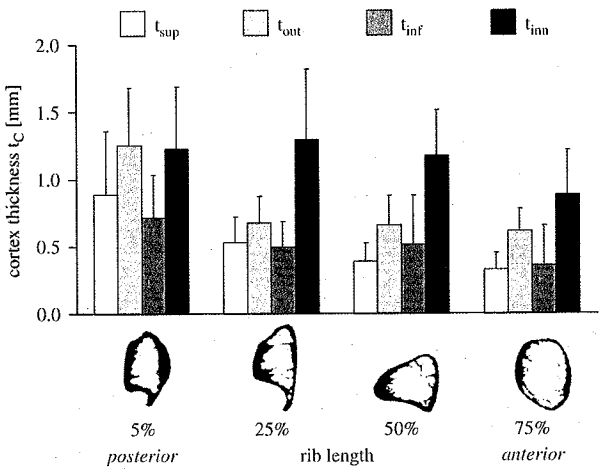

Fig. 5. Average cortical thickness t_C and exemplary cross-sections. Most posteriorly, inner (t_{inn}) and outer (t_{out}) cortex thickness were similar, while from 25% to 75% rib length the inner cortex was the thickest.

significantly by 38% from 29.9 mm^2 at 5% rib length to 41.2 mm^2 at 75% rib length ($p<0.05$).

4. Discussion

The first part of our study concerns the longitudinal geometry of the rib, which so far has mainly been

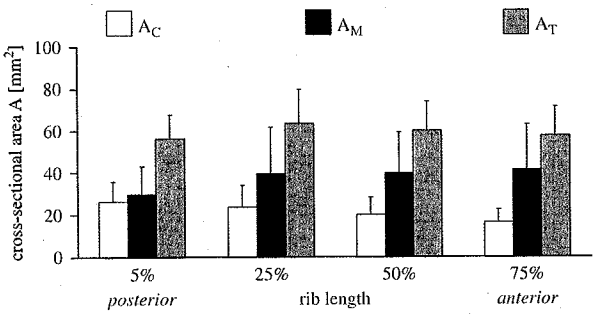

Fig. 6. The total cross-sectional area A_T remained constant along the rib diaphysis. However, the medullary canal area A_M increased and the cortical area A_C decreased from posterior to anterior rib segments.

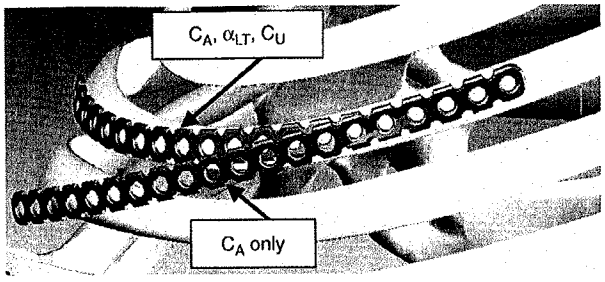

Fig. 7. Contouring a plate to C_A, α_{LT}, and C_U values derived in this study yields a high degree of conformity to the anatomic rib shape, as shown in this example for rib four. In contrast, bending a generic plate to C_A alone will cause the plate to diverge from the rib.

derived from planar projections by the best fitting arc in each rib (Roberts and Chen, 1972; Schultz et al., 1974a, b; Wilson et al., 1987). However, as the curvature of the rib changes over length, this approach provides only rough descriptions of the actual geometry. Schultz et al. (1974a, b) measured ribs two, four, six, and 8–10 of five male cadavers and reported a curvature of $8.9\,m^{-1}$ at rib four and $5.8\,m^{-1}$ at rib eight. Roberts and Chen measured ribs three to ten of one female cadaver. Averaging their results for the superior and inferior border, the shaft curvature varied between $10\,m^{-1}$ at rib three and $5\,m^{-1}$ at rib seven (Roberts and Chen, 1972). Wilson et al. studied CT images of two males measuring the geometrical parameters of ribs 3–7. At functional residual capacity, the curvature ranged from $9.4\,m^{-1}$ for rib three to $7.3\,m^{-1}$ for rib seven (Wilson et al., 1987). These findings correlate with the present study, finding average curvatures of $11.8\,m^{-1}$ for rib three and $8.0\,m^{-1}$ for rib seven. In addition, the data of the current study show that the curvature changes considerably along ribs (Fig. 4). For rib three, the curvature ranged from $17.3\,m^{-1}$ posteriorly to $8\,m^{-1}$ anteriorly. Rib seven ranged from $17.2\,m^{-1}$ posteriorly to $3.8\,m^{-1}$ anteriorly. Dansereau and Stokes (1988) documented the maximum curvature of ribs 2–11 on six cadavers and four volunteers stereoradiographically. As in the current study, the maximum curvature was always measured in the posterior part of the rib and was $28.6\,m^{-1}$ at rib three and $23.6\,m^{-1}$ at rib seven.

For intraoperative plate contouring, the conformity to the longitudinal rib curvature can readily be achieved by out-of-plane bending of osteosynthesis plates, consistent with parameter C_A described in the present study. The longitudinal twist α_{LT} reported in this study provides a novel pre-contouring parameter common to ribs, which can improve the geometric conformity of plates to reduce residual mismatch and stress at the bone–implant interface. Furthermore, this study described the unrolled curvature C_U. This parameter defines an in-plane curvature required for a plate in order to conform to a rib surface upon bending. Intraoperative in-plane bending of osteosynthesis plates is challenging due to their high in-plane flexural rigidity. This finding reflects our clinical observations, whereby conforming of a straight plate to the apparent rib curvature C_A alone causes the plate to gradually migrate off the rib surface (Fig. 7). While apparent rib curvature, unrolled curvature, and magnitude of longitudinal twist can be assumed to be identical for right and left ribs, the direction of twist reverses from counterclockwise for right ribs to clockwise for left ribs, owing to para-sagittal symmetry.

Rib cross-sectional geometry has previously been described. In order to create a finite element model of the thorax, Roberts and Chen determined cortical thickness, cross-sectional area, torsional constant, and moment of inertia in one skeleton (Roberts and Chen, 1970). They showed cortical thickness to increase from anterior to posterior, which was confirmed in our study. While their measurements showed a varying total area, they assumed a constant ratio between cortical area and total area (C/T ratio) of 0.5. Our study has not found significant differences in total area, but characteristic increases in C/T ratio from anterior to posterior in all ribs (range 0.25–0.52). Other studies have investigated cross-sectional geometry in the mid-diaphysis region (Stein and Granik, 1976; Takahashi and Frost, 1966; Yoganandan and Pintar, 1998). Takahashi and Frost (1966) studied age-related changes in cross sections of ribs 5–7 from 326 specimens ranging from 1 week to 90 yr. Their C/T ratio in the age group between 41 and 90 yr (0.33–0.36) correlates well with the results at 50% rib length in ribs 5–7 in the current study (0.34–0.37). Yoganandan and Pintar (1998) measured mid-shaft cross sections of left and right ribs seven and eight in 30 cadavers. Their C/T ratio of rib seven and eight was higher (0.47) than in the current study. The current study presents for the first time a comprehensive quantification of the non-uniform cortex distribution within cross-sections and the changing cross-sectional

properties along the length of the rib and in respect to the anatomical level.

In order to analyze the mechanics of blunt chest trauma, several finite element models of the human thorax have been introduced (Amtmann, 1979; Andriacchi et al., 1974; Roberts and Chen, 1970; Sundaram and Feng, 1977). The mechanical properties of ribs are well known (Cormier et al., 2005; Schultz et al., 1974a, b; Stein and Granik, 1976; Yoganandan and Pintar, 1998). Results of the present study can provide data detailing the longitudinal and cross-sectional geometry for generation of geometrically accurate computational models. In agreement with our findings, Cormier et al. (2005) found rib geometry to vary depending on rib region and level. The present findings that inner and outer cortices are thicker than superior and inferior cortices hold implications for finite element models that employ a uniform cortex thickness (Roberts and Chen, 1970).

This study was limited to ribs 3–9, since these are most amenable to surgical fixation. Surface digitization and physical slicing with subsequent radiographic image analysis were used to derive the desired geometrical parameters. Alternative techniques such as stereo-radiographic reconstruction have been successfully applied by other researchers in three-dimensional rib cage reconstruction (Benameur et al., 2005; Delorme et al., 2003). However, reported errors of $\geqslant 1$ mm in stereo-radiographic and CT-reconstruction procedures would limit the accuracy for assessment of resolution-sensitive outcome parameters, particularly α_{LT} and t_C.

While the geometric congruence of pre-contoured fixation hardware is naturally limited by inter-individual variation in thoracic anatomy, it constitutes a significant improvement over current orthopedic practice. Remaining geometrical incongruence between hardware and fractured bone can be reduced by intraoperative fine adjustment. Alternatively, patient specific implant contouring based on radiographic reconstruction data can deliver the highest congruence. However, this approach is at present not cost-efficient for broad use.

In summary, results delineated the complex rib surface geometry into three basic parameters, which bear direct implications for pre- and intraoperative contouring of osteosynthesis plates used in chest wall fixation. When contouring a straight plate to conform to a rib, sequential application of in-plane bending C_U, longitudinal twist α_{LT}, and apparent rib curvature C_A can provide for a systematic contouring algorithm. Furthermore, results describe for the first time characteristic differences in cortex thickness distribution within rib cross-sections over the rib length. This quantitative information is pertinent to intramedullary fixation of rib fractures and can aid the refinement of computational models of the human thorax.

Acknowledgment

Financial support for this research has been provided by the Legacy Research Foundation.

References

Ahmed, Z., Mohyuddin, Z., 1995. Management of flail chest injury: internal fixation versus endotracheal intubation and ventilation. Journal of Thoracic and Cardiovascular Surgery 110, 1676–1680.

Albrecht, F., Brug, E., 1979. Die zuggurtungsosteosynthese der rippen und des sternums bei instabiler thoraxwand. Zentralblatt fur Chirurgie 104, 770–776.

Amtmann, E., 1979. [Architectonics of the thorax (author's transl)]. Praxis und Klinik der Pneumologie 33, 373–378.

Andriacchi, T., Schultz, A., Belytschko, T., Galante, J., 1974. A model for studies of mechanical interactions between the human spine and rib cage. Journal of Biomechanics 7, 497–507.

Balci, A.E., Eren, S., Cakir, O., Eren, M.N., 2004. Open fixation in flail chest: review of 64 patients. Asian Cardiovascular and Thoracic Annals 12, 11–15.

Benameur, S., Mignotte, M., Destrempes, F., De Guise, J.A., 2005. Three-dimensional biplanar reconstruction of scoliotic rib cage using the estimation of a mixture of probabilistic prior models. IEEE Transactions on Biomedical Engineering 52, 1713–1728.

Boetsch, H., Rehm, K.E., 1981. Biomechanische untersuchungen an rippenosteosynthesen. Biomedizinische Technik 26, 296–301.

Borrely, J., Grosdidier, G., Wack, B., 1985. Surgical treatment of flai chest by sliding staples. Revue de Chirurgie Orthopedique et Reparatrice de L Appareil Moteur 71, 241–250.

Cacchione, R.N., Richardson, J.D., Seligson, D., 2000. Painful nonunion of multiple rib fractures managed by operative stabilization. Journal of Trauma 48, 319–321.

Cormier, J.M., Stitzel, J.D., Duma, S.M., Matsuoka, F., 2005. Regional variation in the structural response and geometrical properties of human ribs. Annual Proceedings, Association for the Advancement of Automotive Medicine 49, 147–164.

Dansereau, J., Stokes, I.A.F., 1988. Measurements of the three dimensional shape of the rib cage. Journal of Biomechanics 21, 893–901.

Delorme, S., Petit, Y., de Guise, J.A., Labelle, H., Aubin, C.E., Dansereau, J., 2003. Assessment of the 3-D reconstruction and high-resolution geometrical modeling of the human skeletal trunk from 2-D radiographic images. IEEE Transactions on Biomedical Engineering 50, 989–998.

Engel, C., Krieg, J.C., Madey, S.M., Long, W.B., Bottlang, M., 2005. Operative chest wall fixation with osteosynthesis plates. Journal of Trauma 58, 181–186.

Fick, R., Bartels, P., Brunn, A., Disse, J., 1911. Handbuch der Anatomie des Menschen. Verlag von Gustav Fischer, Jena, pp. 688.

Friedrich, B., Redeker, H., Kljucar, S., 1991. Die instabile thoraxwand:behandlungsmoeglichkeiten. Helvetica Chirurgica Acta 58, 77–82.

Fujimoto, L.K., Jacobs, G., Przybysz, J., Collins, S., Meaney, T., Smith, W.A., et al., 1984. Human thoracic anatomy based on computed tomography for development of a totally implantable left ventricular assist system. Artificial Organs 8, 436–444.

Haasler, G.B., 1990. Open fixation of flail chest after blunt trauma. Annals of Thoracic Surgery 49, 993–995.

Hellberg, K., de Vivie, E.R., Fuchs, K., Heisig, B., Ruschewski, W., Luhr, H.G., et al., 1981. Stabilization of flail chest by compression osteosynthesis experimental and clinical results. Thoracic and Cardiovascular Surgeon 29, 275–281.

Karev, D.V., 1997. Operative management of the flail chest. Wiad Lek 50, 205–208.

Labitzke, R., 1981. Biomechanic examination of rib plates. Langenbecks Archiv fur Chirurgie 354, 169–171.

Labitzke, R., Schmit-Neuerburg, K.P., Schramm, G., 1980. Indikation zur thoracotomie und rippenstabilisierung beim thoraxtrauma im hohen lebensalter. Chirurg 51, 576–580.

Landercasper, J., Cogbill, T.H., Lindesmith, L.A., 1984. Long-term disability after flail chest injury. Journal of Trauma 24, 410–414.

Landreneau, R.J., Hinson Jr., J.M., Hazelrigg, S.R., Johnson, J.A., Boley, T.M., Curtis, J.J., 1991. Strut fixation of an extensive flail chest. Annals of Thoracic Surgery 51, 473–475.

Lardinois, D., Krueger, T., Dusmet, M., Ghisleta, N., Gugger, M., Ris, H.B., 2001. Pulmonary function testing after operative stabilisation of the chest wall for flail chest. European Journal of Cardiothoracic Surgery 20, 496–501.

Martin, P., Godinou, J.C., Monod, R., Cami, M., Fleury, J.C., Leonard, P., et al., 1982. Costal stapling in severe thoracic traumas. Nouvelle Presse Medicale 11, 851–854.

Mayberry, J.C., Trunkey, D.D., 1997. The fractured rib in chest wall trauma. Chest Surgery Clinics of North America 7, 239–261.

Meier, P., Schuepbach, P., 1978. Zur therapie des instabilen thorax. Schweizerische Medizinische Wochenschrift 108, 608–613.

Menard, A., Testart, J., Philippe, J.M., Grise, P., 1983. Treatment of flail chest with Judets struts. Journal of Thoracic and Cardiovascular Surgery 86, 300–305.

Moore, B.P., 1975. Operative stabilization of nonpenetrating chest injuries. Journal of Thoracic and Cardiovascular Surgery 70, 619–630.

Mouton, W., Lardinois, D., Furrer, M., Regli, B., Ris, H.B., 1997. Long-term follow-up of patients with operative stabilization of a flail chest. Thoracic and Cardiovascular Surgeon 45, 242–244.

Ng, A.B., Giannoudis, P.V., Bismil, Q., Hinsche, A.F., Smith, R.M., 2001. operative stabilisation of painful non-united multiple rib fractures. Injury 32, 637–639.

Nussbaum, M.A., Chaffin, D.B., 1996. Development and evaluation of a scalable and deformable geometric model of the human torso. Clinical Biomechanics 11, 25–34.

Oyarzun, J.R., Bush, A.P., McCormick, J.R., Bolanowski, P.J.P., 1998. Use of 3.5mm acetabular reconstruction plates for internal fixation of flail chest injuries. Annals of Thoracic Surgery 65, 1471–1474.

Quell, M., Vecsei, V., 1991. Surgical stabilization of thoracic wall fractures. Unfallchirurg 94, 129–133.

Reber, P., Ris, H.B., Inderbitzi, R., Stark, B., Nachbur, B., 1993. Osteosynthesis of the injured chest wall. Scandinavian Journal of Thoracic and Cardiovascular Surgery 27, 137–142.

Roberts, S.B., Chen, P.H., 1970. Elastostatic analysis of the human thoracic skeleton. Journal of Biomechanics 3, 527–545.

Roberts, S.B., Chen, P.H., 1972. Global geometric characteristics of typical human ribs. Journal of Biomechanics 5, 191–201.

Schmit-Neuerburg, H., Weiss, H., Labitzke, R., 1982. Indication for thoracotomy and chest wall stabilization. Injury 14, 26–34.

Schultz, A.B., Benson, D.R., Hirsch, C., 1974a. Force-deformation properties of human costo-sternal and costo-vertebral articulations. Journal of Biomechanics 7, 311–318.

Schultz, A.B., Benson, D.R., Hirsch, C., 1974b. Force-deformation properties of human ribs. Journal of Biomechanics 7, 303–309.

Stein, I.D., Granik, G., 1976. Rib structure and bending strength: an autopsy study. Calcified Tissue Research 20, 61–73.

Sundaram, S.H., Feng, C.C., 1977. Finite element analysis of the human thorax. Journal of Biomechanics 10, 505–516.

Takahashi, H., Frost, H.M., 1966. Age and sex related changes in the amount of cortex of normal human ribs. Acta Orthopaedica Scandinavica 37, 122–130.

Tanaka, H., Yukioka, T., Yamaguti, Y., Shimizu, S., Goto, H., Matsuda, H., et al., 2002. Surgical stabilization or internal pneumatic stabilization? A prospective randomized study of management of severe flail chest patients. Journal of Trauma 52, 727–732.

Tscharner, C., Schuepbach, P., Meier, P., Nachbur, B., 1989. Zur operativen behandlung des instabilen thorax bei respiratorischer insuffizienz. Helvetica Chirurgica Acta 55, 711–717.

Vecsei, V., Frenzel, I., Plenk Jr., H., 1979. Eine neue rippenplatte zur stabilisierung mehrfacher rippenbrueche und der thoraxwandfraktur mit paradoxer atmung. Hefte Unfallheilkd 138, 279–282.

Velmahos, G.C., Vassiliu, P., Chan, L.S., Murray, J.A., Berne, T.V., Demetriades, D., 2002. Influence of flail chest on outcome among patients with severe thoracic cage trauma. International Surgery 87, 240–244.

Voggenreiter, G., Neudeck, F., Aufmkolk, M., Obertacke, U., Schmit-Neuerburg, K.P., 1998. Operative chest wall stabilization in flail chest-outcomes of patients with or without pulmonary contusion. Journal of The American College of Surgeons 187, 130–138.

Voggenreiter, G., Neudeck, F., Aufmkolk, M.U.O., Schmit, N., 1996. Behandlungergebnisse der operativen thoraxwandstabilisierung bei instabilem thorax mit und ohne lungenkontusion. Unfallchirurg 99, 425–434.

Wilson, T.A., Rehder, K., Krayer, S., Hoffman, E.A., Whitney, C.G., Rodarte, J.R., 1987. Geometry and respiratory displacement of human ribs. Journal of Applied Physiology 62, 1872–1877.

Yoganandan, N., Pintar, F.A., 1998. Biomechanics of human thoracic ribs. Journal of Biomechanical Engineering 120, 100–104.